Geophysical Research Letters

RESEARCH LETTER
10.1029/2019GL086825

Aerosol Effects on Lightning Characteristics: A Comparison of Polluted and Clean Regimes

Y. Liu[1,2], A. Guha[3], R. Said[4], E. Williams[1], J. Lapierre[5], M. Stock[5], and S. Heckman[5]

[1]Department of Civil and Environmental Engineering, Massachusetts Institute of Technology, Cambridge, MA, USA, [2]Department of Electrical Engineering, Shanghai Jiao Tong University, Shanghai, China, [3]Department of Physics, Tripura University, Agartala, Tripura, India, [4]Vaisala Inc., Louisville, CO, USA, [5]Earth Networks, Germantown, MD, USA

Abstract Oceanic lightning can be a sensitive indicator of aerosol effects on lightning characteristics as thermodynamic contrast is indistinct over adjacent oceanic regions. The study presents discernable aerosol impacts on lightning characteristics by analyzing 2 years (2017–2018) of intracloud (IC) and cloud-to-ground (CG) lightning data from Earth Networks Total Lightning Network over two key regions in southern South China Sea. Mean stroke density, IC/CG ratio, +IC fraction, and +CG fraction in polluted conditions are respectively 3.7, 2, 1.2, and 5.8-fold larger than unpolluted counterparts. Total stroke contrast is further confirmed with the GLD360 network. Thermodynamic parameters conversely support slightly stronger convection over clean ocean. Clear evidence shows cloud droplet size diminishes with added aerosol. Aerosol invigorates more frequent and robust mixed-phase development, endowing maritime convection with continental characteristics. Modifications in the charge reversal temperature and lower and upper positive charge regions are speculated on as means for stimulating more positive ICs and CGs.

Plain Language Summary Over adjacent oceanic regions, the thermodynamic contrast is indistinct, and this makes oceanic lightning a sensitive indicator of aerosol effects. The southern South China Sea, surrounded by wideband electric-field sensors in Earth Networks Total Lightning Network, is focused on the response of both intracloud (IC) and cloud-to-ground (CG) strokes to added aerosol over 2 years (2017–2018). The thermodynamic and cloud microphysical parameters are quantitatively analyzed between polluted and clean oceanic regions. Distribution maps of sulfur dioxide and aerosol optical depth show clear locations for polluted regions. Mean stroke density, IC/CG ratio, +IC fraction, and +CG fraction in polluted conditions are respectively 3.7, 2, 1.2, and 5.8-fold larger than the unpolluted counterparts, while thermodynamic parameters conversely support slightly weaker convection over polluted regions and discount its effects in supporting lightning enhancement. Added aerosol decreases cloud effective particle radius of ice and liquid water based on satellite measurement. Larger lower and upper positive charge reservoirs invigorated by the energized graupel-ice crystal electrification process and possible modification of the charge reversal temperature are speculated as mechanisms to promote more positive strokes. More frequent and robust mixed-phase development favorable for lightning is stimulated by added aerosol over ocean, endowing maritime convection with continental characteristics.

Key Points:
- Oceanic lightning can be a sensitive indicator of aerosol effects on lightning characteristics as the thermodynamic contrast is indistinct or even supports weaker convection in the polluted region
- Mean stroke density, IC/CG ratio, +IC fraction, and +CG fraction in the polluted oceanic region are respectively 3.7, 2, 1.2, and 5.8 -fold larger than the adjacent unpolluted oceanic counterparts
- Aerosol provides for more frequent and robust mixed-phase development, endowing maritime convection with continental characteristics

Supporting Information:
- Supporting Information S1
- Figure S1
- Figure S2
- Figure S3

Correspondence to:
Y. Liu,
yakunliu@mit.edu

Citation:
Liu, Y., Guha, A., Said, R., Williams, E., Lapierre, J., Stock, M., & Heckman, S. (2020). Aerosol effects on lightning characteristics: A comparison of polluted and clean regimes. *Geophysical Research Letters*, *47*, e2019GL086825. https://doi.org/10.1029/2019GL086825

Received 26 DEC 2019
Accepted 4 APR 2020
Accepted article online 17 APR 2020

1. Introduction

Lightning originates from electrification in convective cloud systems and is modulated by cloud dynamics and microphysics (Lang et al., 2004; Rutledge & MacGorman, 1988; Williams et al., 1991). Supercooled liquid water and ice crystals are two essential ingredients for charge separation and thunderstorm electrification, explaining the occurrence of most lightning in the mixed-phase region in the temperature range of 0 to −40°C (Takahashi, 1978; Jayaratne et al., 1983; Williams et al., 1991; Saunders,1993). Convective vigor, hydrometeor size spectrum, and the distribution of these hydrometeors significantly regulate cloud electrification processes, which are influenced by aerosol emitted from plentiful anthropogenic activity across continent and ocean (Altaratz et al., 2010; Wang et al., 2018; Williams, 2020; Williams & Stanfill, 2002). Continental aerosol invigoration is inevitably entangled with pronounced simultaneous thermodynamic alterations. The dominated factor is still to emerge from the combined effects of urban heat island circulation, thermal energy insertion, frictional lift, and aerosol increase over complex terrain (Naccarato et al., 2003; Orville et al., 2001; Westcott, 1995). But in the case of adjacent oceanic regions, the

thermodynamic contrast is indistinct, and its effects can be isolated from aerosol effects, making oceanic lightning a sensitive indicator to assess aerosol effects on lightning characteristics.

Yuan et al. (2011) presented early evidence for aerosol invigoration in maritime convection based on a volcanic eruption case over the west Pacific Ocean. Thornton et al. (2017) have produced key evidence that locally increased aerosol traced to sea container traffic over the Indian Ocean and South China Sea (SCS) can invigorate lightning activity in moist convection. Added aerosol particles participate in cloud microphysical processes by serving as cloud condensation nuclei (CCN) or as ice nuclei and producing numerous smaller cloud droplets with slower coalescence into raindrops. Thus, more liquid water particles are uplifted to become supercooled and in condensing release latent heat in the upper troposphere, which will suppress or delay warm rain formation and enhance convection (Dagan et al., 2015; Mansell & Ziegler, 2013; Ramanathan et al., 2001; Rosenfeld et al., 2008; Rosenfeld & Lensky, 1998; Twomey, 1977).

Aerosol lightning invigoration effects have been documented over different continental and oceanic regions, whereas aerosol effects on lightning characteristics remain inconclusive and in hot debate (Altaratz et al., 2017; Kar et al., 2009; Lyons et al., 1998; Murray et al., 2000; Naccarato et al., 2003; Steiger et al., 2002; Tan et al., 2016). Terrestrial lightning characteristics affected by aerosol are mostly discussed with full utilization of land-based lightning detection networks. A discrepancy is still unresolved in considering the response of the aerosol enhancement in +CG percentage, as some publications show a decrease with rich aerosol loadings in certain urban areas (Kar et al., 2009; Naccarato et al., 2003; Steiger et al., 2002), while other observations show an increase with added aerosol in other urban regions, in smoke-contaminated air (pyrocumulus clouds) and in numerous seasonal biomass fires (Lyons et al., 1998; Murray et al., 2000; Tan et al., 2016). Oceanic lightning is sparse and often distant from land-based detection sensors, leaving few high-resolution lightning data published in this regime. The aforementioned oceanic lightning research was limited to using data from the WWLLN or Lightning Imaging Sensor (LIS) aboard the Tropical Rainfall Measuring Mission (TRMM) satellite, restricting the resolution of lightning characteristics to cloud-to-ground (CG) information alone or total lightning density (Thornton et al., 2017; Yuan et al., 2011).

This study presents 2 years (2017–2018) of quantitative comparisons among lightning characteristics, sulfur dioxide, aerosol optical depth (AOD), and thermodynamic and cloud microphysical parameters over a special marine region in the southern SCS, which is locally polluted by one of the world's busiest shipping lanes. This region is fortunately surrounded by wideband (1 Hz to 12 MHz) electric field sensors of the Earth Networks Total Lightning Network (ENTLN) at distances <700 km, enabling reliable intracloud (IC) and CG stroke information together with their peak current and polarity. The selected oceanic regions are far (>150 km) from coastlines, and their respective areas approach a previously established continental area threshold (~20,000 km^2) for aerosol effects on lightning characteristics (Williams et al., 2004; Williams & Stanfill, 2002).

It is worth mentioning that the misclassified rate for compact IC discharges (CIDs, also known as "narrow bipolar events"), often masquerading as +CGs with high peak current intensity >30 kA in both ENTLN and National Lightning Detection Network observations. The masquerading percentage decreases to 3.7% in ENTLN observations (46.2% in National Lightning Detection Network) for current intensity <30 kA over Florida (Leal et al., 2019). Conservative corrections are made to the +CG stroke analysis for CID contamination by visually examining electric field waveforms from randomly selected +CG events. We show discernable aerosol impacts on lightning characteristics in a background of opposing thermodynamic contrasts and find clear evidence for alterations of cloud microphysics. Aerosol effects on maritime convection and cloud charge structure are discussed to explain these modifications on lightning characteristics.

2. Method and Data

The ENTLN (see https://www.earthnetworks.com) is a unique total lightning detection system and specifically detects the signals emitted from both IC and CG strokes based on over 1,700 wideband electric field sensors deployed in more than 100 countries worldwide (Liu & Heckman, 2011). The ENTLN extends the operational frequency range of detection sensors into the medium frequency and high frequency spectrums to detect weaker discharge pulses at greater distances. These sensors record the entire waveforms of each stroke and transfer them into a central server system for the analysis of lightning parameter by employing sophisticated digital signal processing technologies. The discharge type and polarity are determined by the

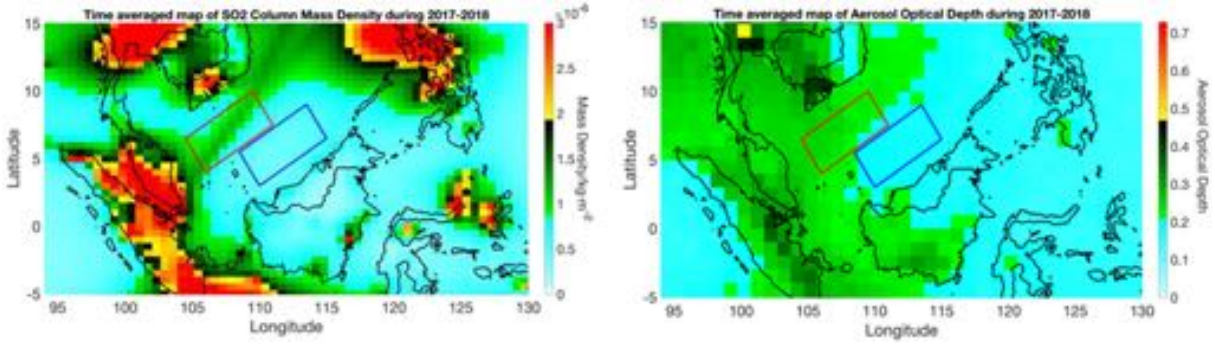

(a) SO_2 column mass density (b) AOD at 550 nm

Figure 1. (a) SO_2 column mass density (spatial resolution 0.5 × 0.625°) and (b) AOD_{550} (spatial resolution 1 × 1°) over the southern SCS during 2017–2018. The polluted oceanic region is marked with a red box. The adjacent pristine oceanic region is marked with a blue box.

sign of the initial half cycle for bipolar pulses and waveform characteristics in the measured electric field (Mallick et al., 2015). Based on ground truthing with natural and rocket-triggered lightning experiments in Florida, the ENTLN processors have a detection efficiency greater than 99% and 96% for flashes and strokes, respectively (Zhu et al., 2017).

The ENTLN established new stations in Asia prior to 2016 and since then has located sensors in Vietnam, Cambodia, Philippines, Indonesia, Singapore, Malaysia, and China. Two years (2017–2018) worth of data over the SCS are selected and analyzed in this study. Compared to the lightning data from the LIS on board the International Space Station in Low Earth Orbit (ISS-LIS), the ENTLN has a high (>90%) and uniform lightning detection efficiency over the entire southern SCS region. CIDs masquerading as +CGs with large peak current portion (>30 kA) will falsely increase +CG density in the statistics and magnify the +CG fractions. Therefore, the electric field waveforms from 120 randomly selected +CG events have been visually examined within six current segments with 10-kA intervals from 0–10 kA, 10–20 kA, ... to >50 kA over the SCS. The misclassification rate is 0%, 10%, 10%, 35%, 70%, and 60% for the six current segments, indicating an overall 3.3% misclassification rate for current intensity <30 kA and consistent with the result of 3.7% found by checking 1022 events over Florida (Leal et al., 2019). To make the most conservative analysis on +CG activity, we make corrections in +CG stroke statistics based on examination of contamination by CIDs in the same manner of Leal et al. (2019).

Air pollutants over the ocean are characterized by measurements of sulfur dioxide (SO_2, a primary indicator for sulfate aerosol) and AOD_{550} (AOD at 550 nm, an aerosol index (Andreae, 2009)). The data on SO_2 concentration, AOD_{550}, cloud base temperature, cloud top height, ice cloud particle effective radius, liquid water cloud particle effective radius, and cloud ice water path (IWP) are all derived from the Moderate Resolution Imaging Spectroradiometer aboard the Sun-synchronous Terra and Aqua platforms (MODIS; Collection 6, Level 3) (Bosilovich et al., 2016; Platnick et al., 2015; Remer et al., 2008). Sea surface temperature (SST) and Convective Available Potential Energy (CAPE) data are collected from the European Centre for Medium-Range Weather Forecasts interim reanalysis database (ERA-Interim, ECMWF) (Berrisford et al., 2009).

3. Results and Discussion

SO_2 is the primary gaseous indicator for diesel engine ship exhaust. AOD_{550} measurements quantify the amount of aerosol present in the atmosphere as an aerosol index (Andreae, 2009). Figure 1 shows the biennial mean SO_2 column mass density and AOD_{550} distribution over the southern SCS. One region of interest with an obvious pollutant track attributed to ship exhaust (enclosed in red in Figure 1) and its adjacent pristine region in parallel (with same area, enclosed in blue) are focused on to compare lightning characteristics and analyze its seasonal variations. These two selected regions are in similar homogeneous meteorological conditions and free from the influences of the diurnal circle in sea breezes and terrain-induced convergence (Thornton et al., 2017). Results show biennially averaged SO_2 column mass density increases to ~2 times

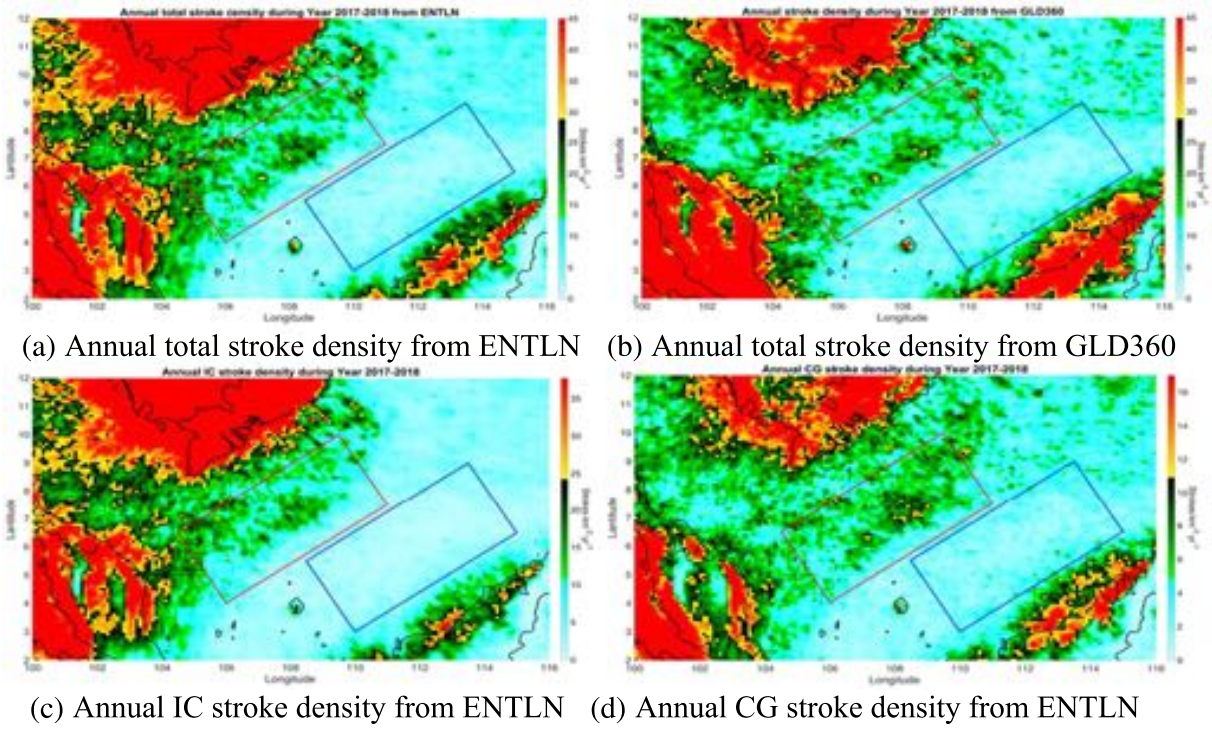

Figure 2. Annual stroke density from (a) ENTLN and (b) GLD360, (c) annual IC stroke density and (d) annual CG stroke density from ENTLN over the southern SCS during 2017–2018. The polluted oceanic region is marked with a red box. Its adjacent pristine ocean region is marked with a blue box.

over the polluted region. AOD_{550} changes from a value of 0.19 on average over the clean region to an average of 0.26 over the polluted region, suggesting an addition of ~270 cm^{-3} in CCN concentrations at a supersaturation of 0.4% over the polluted region (Andreae, 2009; Rosenfeld et al., 2008).

Lightning characteristics over the two oceanic regions are summarized by integrating results from the biennial ENTLN lightning data. The annual IC and CG density distribution is plotted on 0.1° × 0.1° grids and shown in Figure 2. The ENTLN lightning data show that total stroke number over the polluted region is 3.7-fold greater than that over the adjacent clean region. Annual IC and CG densities are 9.7 and 5.3 strokes·km^{-2}·yr^{-1} over the polluted region, enhanced by 5.1-fold and 2.5-fold compared with the clean region, respectively, and consistent with the lightning contrast 2 times higher for the polluted ocean according to the WWLLN observation (mainly detecting CGs) (Thornton et al., 2017). Thornton et al. (2017) showed that the mean annual lightning density increases quasi-linearly from 0.8 to 1.4 strokes·km^{-2}·yr^{-1} during 2005–2011 and accelerates to 2.3 strokes·km^{-2}·yr^{-1} during 2011–2016 with steeper gradient (partially due to the increasing detection efficiency of WWLLN). The CG stroke density is 5.3 strokes·km^{-2}·yr^{-1} during 2017–2018 in checking the ENTLN lightning data. This variation can be understood by consideration of both the aerosol enhancement and the higher detection efficiency of the ENTLN compared with the WWLLN. The mean IC/CG ratio is 1.9 over the polluted region and enhanced by a factor of 2 compared with the clean region. +IC strokes account for 75% of the total IC strokes over the polluted region and 62% over the clean region. The +CG fraction of total CGs changes substantially to 6.4% over the polluted region from 1.1% in the clean condition.

Lightning observations from the global very low frequency network GLD360 have also been utilized to make a further confirmation of the contrast in total stroke density over the polluted and clean regions defined by the shipping lane in the SCS. The findings here corroborate the earlier results found with the World Wide Lightning Location Network (WWLLN) by Thornton et al. (2017), but in both cases, no classification of ICs and CGs is available. GLD360 detects the global lightning with numerous very low frequency sensors strategically placed around the world (Said et al., 2010). The GLD360 data show that the total annual stroke density over the polluted region is 18.1 strokes·km^{-2}·yr^{-1} (compared with 15 strokes·km^{-2}·yr^{-1} for ENTLN,

and ~2.3 strokes·km^{-2}·yr^{-1} for WWLLN), which is 2.2-fold greater than that over the adjacent clean region during the year 2017–2018. Figures 2a and 2b show a good agreement between ENTLN and GLD360 on the total stroke density over the polluted and clean regions, for which the correlation coefficient for the stroke density is 0.8 over the polluted region and 0.9 over the clean region. The stroke densities from both the ENTLN and GLD360 data sets are much higher than the earlier result of WWLLN (Thornton et al., 2017) and exhibit a substantial enhancement over the polluted region, although there is a modest difference in lightning detection efficiency between the GLD360 and ENTLN.

In Figures 2c and 2d, the IC and CG stroke density shows a pronounced enhancement within the shipping lane previously characterized (see Figure 1) with elevated SO_2 column mass density and AOD_{550}. This enhancement is further confirmed by checking the lightning density maps and aerosol indicators during the seasons of active convection (see Figure S1 in the supporting information, which shows satisfactory consistency with the analyses on the annual timescale). The mean IC stroke density is 1.9-fold higher than the CG stroke density over the polluted region. Both ICs and CGs are invigorated at scales smaller than the size of the enclosing box and within the maximum pollutants. The highest IC and CG densities can reach 23 and 14.2 strokes·km^{-2}·yr^{-1} over the polluted region, while the highest IC and CG densities over the clean region are 7.4 and 7.2 strokes·km^{-2}·yr^{-1}, respectively.

The maximum lightning enhancement lies near the center of the enclosing pollutant box. And clearly, some gaps with fewer IC and CG strokes are observed between the polluted shipping lane and the coastline, suggesting there is little influence on lightning activity from continent or coasts. Lightning over the selected clean region is sparse and quantitatively consistent with other open oceanic regions in the southern SCS. This aerosol perturbation on lightning activity seems to concentrate locally and does not disturb the neighboring regions, which can be explained by the rapid aerosol dilution with distance in the open ocean and the large area (20,000–30,000 km^2) required for aerosol influence on lightning (Williams et al., 2004).

Figure 3a shows the monthly variation of annual lightning density averaged within the polluted region and its adjacent clean region during 2017–2018. Both IC and CG activities exhibit seasonal cycles influenced by the meridional migration of the intertropical convergence zone and the monsoon system (Hu et al., 2000; Waliser & Gautier, 1993), indicating this lightning enhancement is not caused by coincident contributions from some extremely active anomalies. During the wet season (May to October), lightning increases significantly and consistently over the polluted region, although mean monthly statistics indicate that the clean ocean is 0.1 K warmer in SST and 77 J/kg stronger in CAPE and support slightly stronger convection over the clean ocean, as shown in Figures 3b and 3c. This weak contrast in thermodynamic conditions between adjacent ocean regions might be understood with drizzle reduction by added aerosol, with consequent increase in the amount of low-level cloudiness and regional albedo to enhance reflectivity associated with a cooler sea surface (Albrecht, 1989). Cloud base temperature shows little contrast (<1%) between the polluted and clean regions. Cloud top height is ~5% higher over the clean region than the polluted condition. These comparisons discount thermodynamic effects in supporting the observed lightning enhancement over the polluted oceanic region.

During the dry season (November to April), mean monthly contrasts of SST and CAPE amplify to a peak of 1.6 K warmer in SST and 357 J/kg stronger in CAPE over the clean region (Figures 3b and 3c), suggesting the updraft and vertical convection are stronger over the clean region. The intertropical convergence zone subsidence suppresses the vertical convections above the boundary level and also restrains aerosol being uplifted above the cloud base. In addition, wind speed increases sharply in episodes known as cold surges during the northeast monsoon season (December to March) (Wang et al., 2009). Strong horizontal wind surges can efficiently dilute aerosol and decrease its concentration for unit volume in cold seasons. These circumstances during the dry season restrain aerosol effects and build up the foundation for a slightly more lightning over the clean region (Figure 3a).

Whereas lightning enhancement can still be observed in some months during the dry season, such as April in 2017, November and December in 2018, those are competing results between thermodynamic effects and aerosol effects. If we calculate the resultant released CAPE for a cloud parcel ascending to the tropopause induced by added aerosol using the modeling calculation involving AOD, CCN, and CAPE (Rosenfeld et al., 2008), the AOD change from 0.2 to 0.3 can bring an increase in CAPE of 300 J/kg. This modeling relationship linking AOD and CAPE can readily explain the monthly lightning contrasts during the dry season

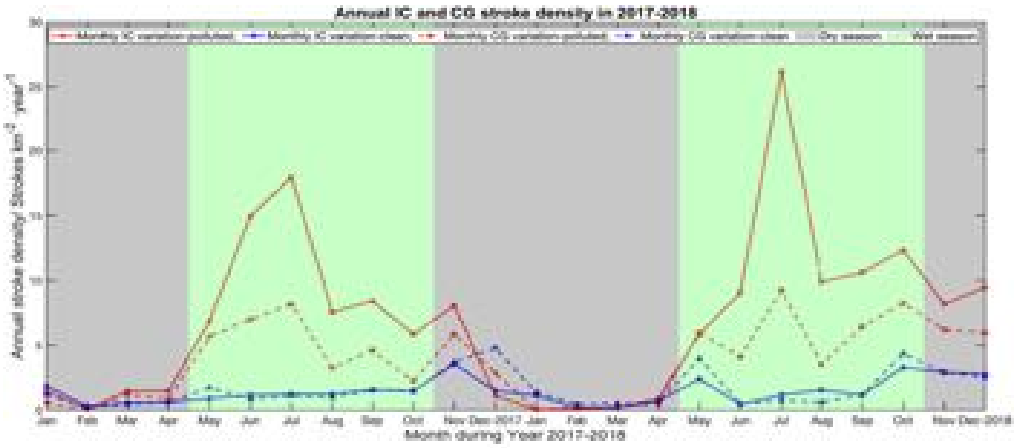

(a) Monthly variations of the ENTLN annual IC and CG stroke density averaged within the polluted region (red line for ICs and red dashed line for CGs) and its adjacent clean region (blue line for IC strokes and blue dashed line for CG strokes) during 2017-2018.

(b) Monthly variations of SST averaged within the polluted region (red line with ±50% standard deviation at each data point within the region) and its adjacent clean region (blue line with ±50% standard deviation at each data point within the region) during 2017-2018.

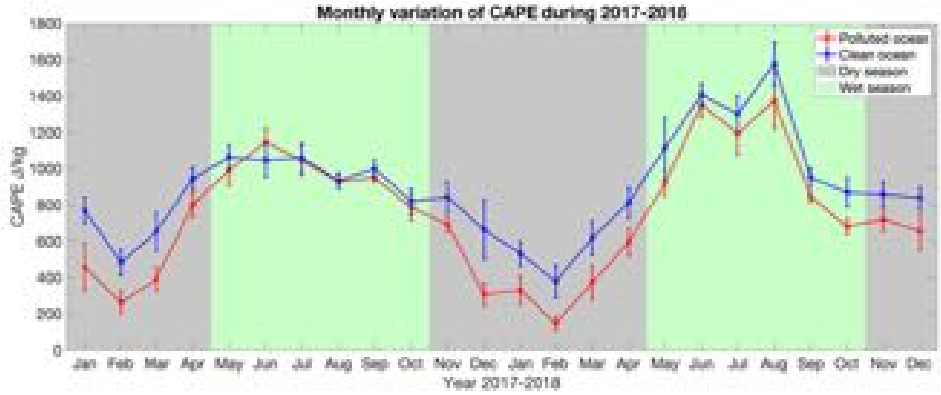

(c) Monthly variations of CAPE averaged within the polluted region (red line with ±50% standard deviation at each data point within the region) and its adjacent clean region (blue line with ±50% standard deviation at each data point within the region) during 2017-2018.

Figure 3. Monthly variations of (a) ENTLN annual lightning stroke density, (b) SST, (c) CAPE, (d) AOD_{550}, (e) SO_2 column mass density, cloud particle effective radius of (f) ice and (g) liquid water, and (h) ice water path averaged within the polluted region (red line), and its adjacent clean region (blue line) during 2017–2018. Time periods filled with the light gray color show the dry season and the light green color show the wet season.

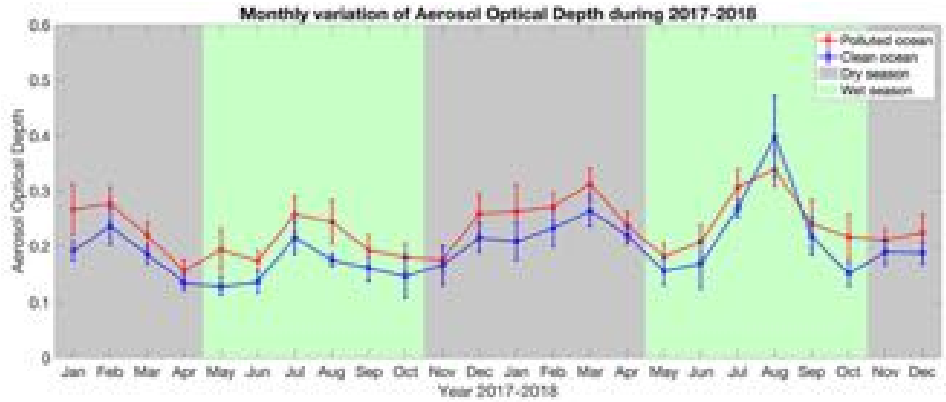

(d) Monthly variations of AOD_{550} averaged within the polluted region (red line with ±50% standard deviation at each data point within the region) and its adjacent clean region (blue line with ±50% standard deviation at each data point within the region) during 2017-2018.

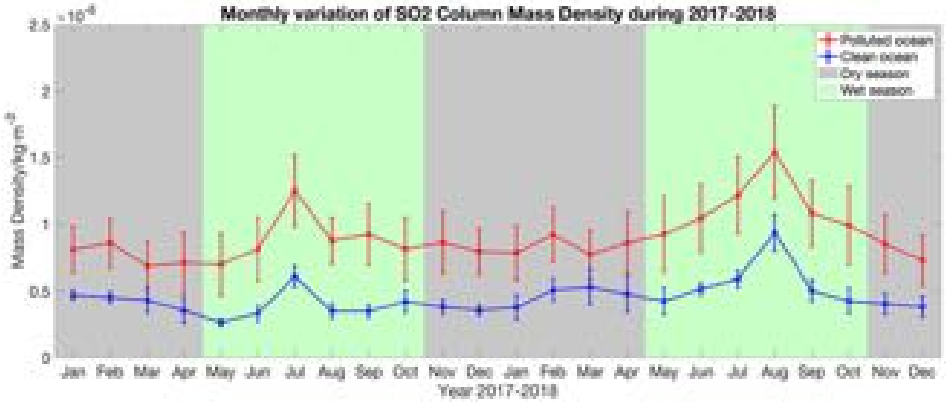

(e) Monthly variations of the SO_2 column mass density averaged within the polluted region (red line with ±50% standard deviation at each data point within the region) and its adjacent clean region (blue line with ±50% standard deviation at each data point within the region) during 2017-2018.

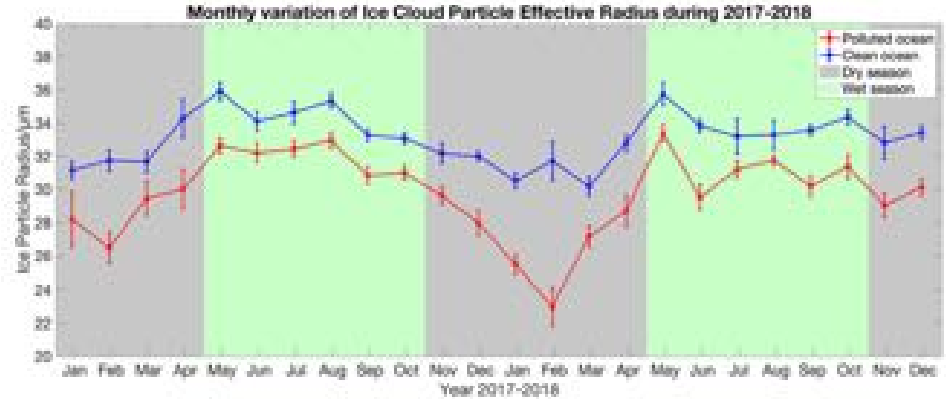

(f) Monthly variations of the ice cloud particle effective radius averaged within the polluted region (red line with ±50% standard deviation at each data point within the region) and its adjacent clean region (blue line with ±50% standard deviation at each data point within the region) during 2017-2018.

Figure 3. *(Continued)*

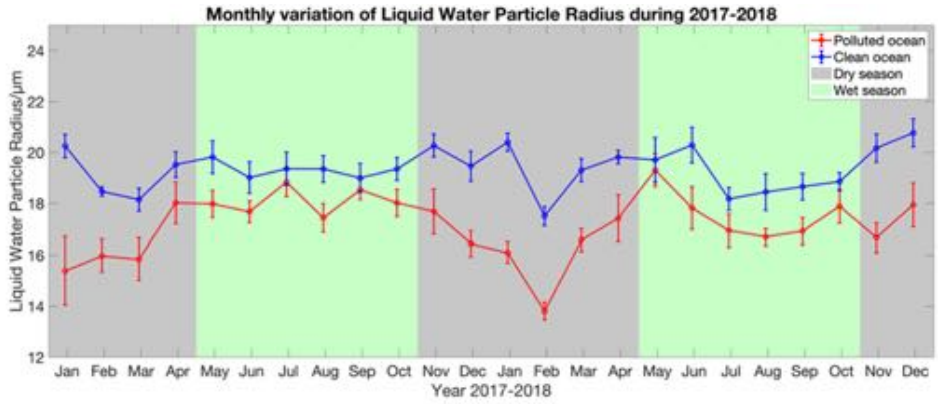

(g) Monthly variations of the liquid water cloud particle effective radius averaged within the polluted region (red line with ±50% standard deviation at each data point within the region) and its adjacent clean region (blue line with ±50% standard deviation at each data point within the region) during 2017-2018.

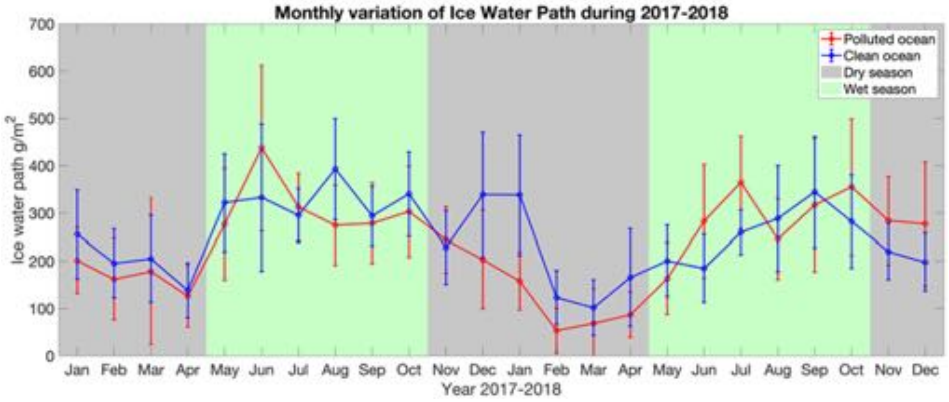

(h) Monthly variations of Ice Water Path averaged within the polluted region (red line with ±50% standard deviation for each data point within the region) and its adjacent clean region (blue line with ±50% standard deviation at each data point within the region) during 2017-2018.

Figure 3. *(Continued)*

affected by competing thermodynamic and aerosol effects. Meanwhile, monthly data on SO_2 column mass density and AOD_{550} have also been examined. Results (Figures 3d and 3e) show stably higher values over the polluted region and an obvious peak appears in July/August. Interestingly, an apparent peak for lightning density is also observed in July/August. AOD_{550} data show an anomaly in the spike in August 2018 over the clean region (As shown by the Figures S2 and S3, this anomaly is caused by aerosol emanating from a strong pollution source over the land near West Kalimantan, Indonesia.). We can observe an associated slight IC stroke enhancement in August from the variations of the monthly lightning density over the clean oceanic region, but this enhancement is not observed in August 2017 (see Figure 3a).

Lightning activity is invigorated over the polluted region even when synoptic thermodynamic parameters support weaker convection compared to the clean region. The aerosol hypothesis (Rosenfeld et al., 2008) is speculated to account for this lightning enhancement. We checked cloud microphysics parameters and results (Figures 3f and 3g) that show cloud particle effective radius of ice and liquid water are smaller over the polluted ocean, consistent with the observed decrease of cloud particle size in Yuan et al. (2011) and Sherwood et al. (2006). This supports the idea that aerosol reduces the cloud droplet size spectrum. Nucleating numerous smaller droplets can slow the coalescence rate into raindrops and suppress the warm rain from convective clouds (Guo et al., 2016; Rosenfeld et al., 2008), thereby supplying more cloud liquid

water to the mixed-phase region to provide rime for ice hydrometeors (i.e., graupel and hail). The monthly variations of mean IWP exhibit a noticeable enhancement over the polluted region during the wet season (Figure 3h), even though the polluted region manifests a weaker thermodynamic state in CAPE and SST compared with the clean region (Figures 3b and 3c). This enhancement associated with lightning invigoration is consistent with the invariant positive correlation between IWP and flash density across land and ocean (Deierling et al., 2008; Petersen et al., 2005).

More supercooled liquid water and more numerous ice crystals can increase the charging in the noninductive charge separation process as demonstrated in the simulated riming electrification experiments of Takahashi (1978) and Saunders (1993) in the laboratory. Additionally, more cloud liquid water with smaller droplets can intensify convection by releasing more latent heat in ascent to the freezing level and reabsorbing heat at lower levels where ice particles melt, providing for more noninductive charge separations per unit mass in comparison with the unpolluted condition with larger cloud droplets (Rosenfeld & Woodley, 2000; Williams et al., 1999; Yuan et al., 2011).

It is worth mentioning that lightning activity is not expected to increase monotonically with the addition of aerosol. Altaratz et al. (2010) and Wang et al. (2018) showed a robust and consistent "boomerang trend" for the relationship between lightning counts and AOD with a tipping point at an AOD value of ~0.3 (for the year 2009 with a better detection efficiency of WWLLN in Altaratz et al., 2010). The simulation of aerosol effects on electrification and precipitation (Mansell & Ziegler, 2013) suggests that charge separation and lightning activity increase with the concentration of CCN up to the threshold of 2,000 cm^{-3}. Beyond this threshold, ice crystal concentration declines radically with a reduced availability in the number of large cloud droplets effective for rime-splintering ice multiplication. An AOD value of ~0.3 at the tipping point corresponds to a $CCN_{0.4}$ concentration of 2,000 cm^{-3}. In this study, AOD_{550} values vary within the range 0.19–0.26 over regions, suggesting an increase from ~800 cm^{-3} to ~1070 cm^{-3} in $CCN_{0.4}$ (Rosenfeld et al., 2008). The magnified $CCN_{0.4}$ concentrations caused by pollutants are still lower than the threshold and support an increased response of lightning to added aerosol. Although a good agreement is found between the observational results and modeling analyses for the role of aerosol on lightning activity, attention should be paid as the simulations cannot fully represent the natural results due to limitations related to incomplete inputs and some unresolved physical problems.

Lightning contrasts in annual IC stroke density and positive IC and CG stroke densities over the polluted and clean regions exhibit apparent elevations relative to an enhancement of 3.7-fold in total stroke density. These quantities are increased respectively to 5.1, 6.0, and 14.7 times. This implies aerosol effects are not in a proportional stimulation pattern in consideration of lightning types. Relatively larger number of normal IC discharges and positive discharges (both ICs and CGs) occur. IC discharges are enhanced primarily by more frequent and more robust mixed-phase development favorable for lightning, as the systematic vigor of maritime convective clouds is stimulated by the added aerosol (Koren et al., 2005). Meanwhile, more robust mixed-phase development over the polluted oceanic region can result in higher charge density in the "normal" tripole charge structure (Williams, 1989), thereby promoting greater IC activity and a larger lower positive charge reservoir. The larger reservoir could also facilitate some attempted CG leaders evolving into ICs by preventing the descending negative leader from reaching ground (Nag & Rakov, 2009, figure 3; Cui et al., 2009; Nag & Rakov, 2012). This candidate mechanism needs to be further confirmed with a valuable ship-board polarimetric radar campaign over the polluted and clean regions.

More liquid water and larger numbers of ice crystals above the freezing level caused by added aerosol motivate the formation of a larger lower positive charge reservoir. This scenario may be validated by the vertical profiles of radar reflectivity with height. Unfortunately, the TRMM Precipitation Radar (PR) was decommissioned in 2015, and no land-based radar data are available over this ocean region during 2017–2018. But the addition of liquid water and ice crystal content can be inferred from the indirect evidence of the vertical radar reflectivity profiles from the TRMM PR over volcano-polluted ocean in the year 2005 (Yuan et al., 2011, figure 4), the TRMM PR vertical radar reflectivity anomalies over oceanic ship tracks (Thornton et al., 2017, figure 4), and the slower decreases in vertical profiles of radar reflectivity (Stolz et al., 2014, figure 12) over oceanic lightning-prone regions. Spectral microphysics mixed-phase cloud model analysis (Khain et al., 2008) also shows that aerosols crossing maritime cloud base will cause a significant increase in the amount of supercooled water, ice crystals, and vertical velocities. All these findings support the appearance of more

ice crystals above the 0°C isotherm. Thus, stronger graupel-ice cloud electrification will take place and form a more vigorous lower positive charge structure. For testing this hypothesis, a ship-board polarimetric radar campaign is urgently needed to study the cloud microphysics over the polluted and clean regions in the SCS.

Laboratory riming electrification experiments have shown that both chemical contamination of cloud droplets and the cloud-droplet spectrum can remarkably influence the charge reversal temperature in the noninductive charging (Avila et al., 1999; Jayaratne et al., 1983; Saunders, 1993). The chemical composition from seagoing ship exhaust consists mainly of carbon oxide, organic, ammonium, sulfate, nitrate, and other compounds (Murphy et al., 2009). Added aerosol influences the cloud electrification process with more impurities in the cloud water and a smaller particle size spectrum. The spectrum of small droplets encourages positive graupel charging in a temperature range −10°C to −25°C in contrast to charging negatively at temperature below −18°C for a larger droplet spectrum (Avila et al., 1999), suggesting that the lower positive charge region may strengthen and extend to higher altitude (Naccarato et al., 2003). Na^+ and Cl^- ion concentration in cloud water is typically 10^{-4} N in clouds over the ocean (larger than 10^{-5} N over land) and make graupel charge negatively at temperature −6°C to −20°C in experiments (Jyaratne et al., 1983). This may account for the higher negative stroke fraction over clean ocean. But added ammonia sulfate from ship exhaust can support charging positively. Meanwhile, all input aerosol contamination will shift the droplet size spectrum to smaller sizes (Jayaratne et al.1983). The findings on changes in lightning type in polluted conditions suggest a stronger lower and upper positive charge region that may cause a higher ratio of positive discharges over the polluted ocean than clean ocean.

4. Summary and Conclusions

The earlier findings of Thornton et al. (2017) pertaining to oceanic shipping lanes are confirmed with two additional lightning detection networks (ENTLN and GLD360), the first of which enables a comparison of lightning characteristics over adjacent ocean regions. These comparisons supply unique conditions to disentangle the contributions of aerosols and thermodynamics to lightning. Furthermore, added aerosol can contribute to a cooler sea surface and weaker CAPE to suppress thermodynamic effects on lightning and make oceanic lightning a sensitive indicator for aerosol effects. The biennial validation over the localized polluted ocean with ENTLN observations shows that mean stroke density, IC stroke density, CG stroke density, +IC, and +CG stroke densities increase respectively by 3.7, 5, 2.5, 6.0, and 14.7-fold in comparison with the adjacent clean counterpart. More cloud liquid water particles and ice crystals are nucleated with a diminished droplet size spectrum in the cloud convective system. Systematic vigor of maritime convective clouds is stimulated by added aerosol to boost more frequent and robust mixed-phase development favorable for lightning. Larger lower and upper positive charge structures invigorated by the energized graupel-ice crystal electrification process and possible modification of the charge reversal temperature are speculated as a mechanism for promoting more positive strokes. The IC/CG ratio and +CG fraction in total CGs increases substantially to 1.9% and 6.4% over the polluted ocean. Aerosol appears to endow the maritime convection with continental characteristics in both cloud microphysical and lightning categories.

Acknowledgments
The authors thank Adonis Leal, Vlad Rakov, Joan Montanya, Mohd Riduan Ahmad, and Martin Wolf for their helpful discussion and improvement on this paper. This work would not have been accomplished without the valuable lightning data from ENTLN (www.earthnetworks.com/product/weather-sensors/lightning/) and GLD360 (www.vaisala.com/en/products/data-subscriptions-and-reports/data-sets/gld360), the thermodynamic and cloud microphysics data from the MODIS (https://search.earthdata.nasa.gov/search), and ERA-Interim, ECMWF (https://apps.ecmwf.int/datasets/data/interim-full-moda/levtype=sfc/). Thanks to two anonymous reviewers and the editor whose constructive comments contributed to the improvement of this manuscript.

References

Albrecht, B. A. (1989). Aerosols, cloud microphysics, and fractional cloudiness. *Science*, *245*(4923), 1227–1230. https://doi.org/10.1126/science.245.4923.1227

Altaratz, O., Koren, I., Yair, Y., & Price, C. (2010). Lightning response to smoke from Amazonian fires. *Geophysical Research Letters*, *37*(7), L07801–L07806. https://doi.org/10.1029/2010GL042679

Altaratz, O., Kucienska, B., Kostinski, A., Raga, G. B., & Koren, I. (2017). Global association of aerosol with flash density of intense lightning. *Environmental Research Letters*, *12*(11), 114037. https://doi.org/10.1088/1748-9326/aa922b

Andreae, M. O. (2009). Correlation between cloud condensation nuclei concentration and aerosol optical thickness in remote and polluted regions. *Atmospheric Chemistry and Physics*, *9*(2), 543–556. https://doi.org/10.5194/acp-9-543-2009

Avila, E. E., Pereyra, R. G., Varela, G. A., & Caranti, G. M. (1999). The effect of the cloud-droplet spectrum on electrical-charge transfer during individual ice-ice collisions. *Quarterly Journal of the Royal Meteorological Society*, *125*(557), 1669–1679. https://doi.org/10.1002/qj.49712555709

Berrisford, P., Dee, D. P. K. F., Fielding, K., Fuentes, M., Kallberg, P., Kobayashi, S., & Uppala, S. (2009). The ERA-interim archive, ERA report series. *1*, 1–16. http://www.ecmwf.int/publications/library/do/refer

Bosilovich, M. G., Lucchesi, R., & Suarez, M. (2016). MERRA-2: File Specification. *GMAO Office Note No. 9* (Version 1.1), 73 pp, available from http://gmao.gsfc.nasa.gov/pubs/office_notes.

Cui, H., Qie, X., Zhang, Q., Zhang, T., Zhang, G., & Yang, J. (2009). Intracloud discharge and the correlated basic charge structure of a thunderstorm in Zhongchuan, a Chinese Inland Plateau region. *Atmospheric Research*, *91*(2–4), 425–429. https://doi.org/10.1016/j.atmosres.2008.06.007

Dagan, G., Koren, I., & Altaratz, O. (2015). Aerosol effects on the timing of warm rain processes. *Geophysical Research Letters*, *42*(11), 4590–4598. https://doi.org/10.1002/2015GL063839

Deierling, W., Petersen, W. A., Latham, J., Ellis, S., & Christian, H. J. (2008). The relationship between lightning activity and ice fluxes in thunderstorms. *Journal of Geophysical Research*, *113*(D15). https://doi.org/10.1029/2007JD009700

Guo, J., Deng, M., Lee, S. S., Wang, F., Li, Z., Zhai, P., et al. (2016). Delaying precipitation and lightning by air pollution over the Pearl River Delta. Part I: Observational analyses. *Journal of Geophysical Research: Atmospheres*, *121*(11), 6472–6488. https://doi.org/10.1002/2015JD023257

Hu, J., Kawamura, H., Hong, H., & Qi, Y. (2000). A review on the currents in the South China Sea: Seasonal circulation, South China Sea warm current and Kuroshio intrusion. *Journal of Oceanography*, *56*(6), 607–624. https://doi.org/10.1023/A:1011117531252

Jayaratne, E. R., Saunders, C. P. R., & Hallett, J. (1983). Laboratory studies of the charging of soft-hail during ice crystal interactions. *Quarterly Journal of the Royal Meteorological Society*, *109*(461), 609–630. https://doi.org/10.1002/qj.49710946111

Kar, S. K., Liou, Y. A., & Ha, K. J. (2009). Aerosol effects on the enhancement of cloud-to-ground lightning over major urban areas of South Korea. *Atmospheric Research*, *92*(1), 80–87. https://doi.org/10.1016/j.atmosres.2008.09.004

Khain, A., Cohen, N., Lynn, B., & Pokrovsky, A. (2008). Possible aerosol effects on lightning activity and structure of hurricanes. *Journal of the Atmospheric Sciences*, *65*(12), 3652–3677. https://doi.org/10.1175/2008JAS2678.1

Koren, I., Kaufman, Y. J., Rosenfeld, D., Remer, L. A., & Rudich, Y. (2005). Aerosol invigoration and restructuring of Atlantic convective clouds. *Geophysical Research Letters*, *32*(14), L14828. https://doi.org/10.1029/2005GL023187

Lang, T. J., Miller, L. J., Weisman, M., Rutledge, S. A., Barker, L. J. III, Bringi, V. N., et al. (2004). The severe thunderstorm electrification and precipitation study. *Bulletin of the American Meteorological Society*, *85*(8), 1107–1126. https://doi.org/10.1175/BAMS-85-8-1107

Leal, A. F., Rakov, V. A., & Rocha, B. R. (2019). Compact intracloud discharges: New classification of field waveforms and identification by lightning locating systems. *Electric Power Systems Research*, *173*, 251–262. https://doi.org/10.1016/j.epsr.2019.04.016

Liu, C., & Heckman, S. (2011). The application of total lightning detection and cell tracking for severe weather prediction. In 91st American Meteorological Society Annual Meeting, Seattle, WA.

Lyons, W. A., Nelson, T. E., Williams, E. R., Cramer, J. A., & Turner, T. R. (1998). Enhanced positive cloud-to-ground lightning in thunderstorms ingesting smoke from fires. *Science*, *282*(5386), 77–80. https://doi.org/10.1126/science.282.5386.77

Mallick, S., Rakov, V. A., Hill, J. D., Ngin, T., Gamerota, W. R., Pilkey, J. T., et al. (2015). Performance characteristics of the ENTLN evaluated using rocket-triggered lightning data. *Electric Power Systems Research*, *118*, 15–28. https://doi.org/10.1016/j.epsr.2014.06.007

Mansell, E. R., & Ziegler, C. L. (2013). Aerosol effects on simulated storm electrification and precipitation in a two-moment bulk microphysics model. *Journal of the Atmospheric Sciences*, *70*(7), 2032–2050. https://doi.org/10.1175/JAS-D-12-0264.1

Murphy, S. M., Agrawal, H., Sorooshian, A., Padró, L. T., Gates, H., Hersey, S., et al. (2009). Comprehensive simultaneous shipboard and airborne characterization of exhaust from a modern container ship at sea. *Environmental Science & Technology*, *43*(13), 4626–4640. https://doi.org/10.1021/es802413j

Murray, N. D., Orville, R. E., & Huffines, G. R. (2000). Effect of pollution from Central American fires on cloud-to-ground lightning in May 1998. *Geophysical Research Letters*, *27*(15), 2249–2252. https://doi.org/10.1029/2000GL011656

Naccarato, K. P., Pinto, O. Jr., & Pinto, I. R. C. A. (2003). Evidence of thermal and aerosol effects on the cloud-to-ground lightning density and polarity over large urban areas of Southeastern Brazil. *Geophysical Research Letters*, *30*(13), 1674. https://doi.org/10.1029/2003GL017496

Nag, A., & Rakov, V. A. (2009). Some inferences on the role of lower positive charge region in facilitating different types of lightning. *Geophysical Research Letters*, *36*(5). https://doi.org/10.1029/2008GL036783

Nag, A., & Rakov, V. A. (2012). Positive lightning: An overview, new observations, and inferences. *Journal of Geophysical Research*, *117*(D8), D08109 1–D08109 20. https://doi.org/10.1029/2012JD017545

Orville, R. E., Huffines, G., Nielsen-Gammon, J., Zhang, R., Ely, B., Steiger, S., et al. (2001). Enhancement of cloud-to-ground lightning over Houston, Texas. *Geophysical Research Letters*, *28*(13), 2597–2600. https://doi.org/10.1029/2001GL012990

Petersen, W. A., Christian, H. J., & Rutledge, S. A. (2005). TRMM observations of the global relationship between ice water content and lightning. *Geophysical Research Letters*, *32*(14). https://doi.org/10.1029/2005GL023236

Platnick, S., Ackerman, S. A., King, M. D., Meyer, K., Menzel, W. P., Holz, R. E., et al. (2015). *MODIS Atmosphere L2 Cloud Product (06_L2). NASA MODIS Adaptive Processing System*. USA: NASA Goddard Space Flight Center. https://doi.org/10.5067/MODIS/MOD06_L2.006

Ramanathan, V. C. P. J., Crutzen, P. J., Kiehl, J. T., & Rosenfeld, D. (2001). Aerosols, climate, and the hydrological cycle. *Science*, *294*(5549), 2119–2124. https://doi.org/10.1126/science.1064034

Remer, L. A., Kleidman, R. G., Levy, R. C., Kaufman, Y. J., Tanré, D., Mattoo, S., et al. (2008). Global aerosol climatology from the MODIS satellite sensors. *Journal of Geophysical Research*, *113*(D14). https://doi.org/10.1029/2007JD009661

Rosenfeld, D., & Lensky, I. M. (1998). Satellite-based insights into precipitation formation processes in continental and maritime convective clouds. *Bulletin of the American Meteorological Society*, *79*(11), 2457–2476. https://doi.org/10.1175/1520-0477(1998)079<2457:SBIIPF>2.0.CO;2

Rosenfeld, D., Lohmann, U., Raga, G. B., O'Dowd, C. D., Kulmala, M., Fuzzi, S., et al. (2008). Flood or drought: How do aerosols affect precipitation? *Science*, *321*(5894), 1309–1313. https://doi.org/10.1126/science.1160606

Rosenfeld, D., & Woodley, W. L. (2000). Deep convective clouds with sustained supercooled liquid water down to −37.5°C. *Nature*, *405*(6785), 440–442. https://doi.org/10.1038/35013030

Rutledge, S. A., & MacGorman, D. R. (1988). Cloud-to-ground lightning activity in the 10–11 June 1985 mesoscale convective system observed during the Oklahoma–Kansas PRE-STORM project. *Monthly Weather Review*, *116*(7), 1393–1408. https://doi.org/10.1175/1520-0493(1988)116<1393:CTGLAI>2.0.CO;2

Said, R. K., Inan, U. S., & Cummins, K. L. (2010). Long-range lightning geolocation using a VLF radio atmospheric waveform bank. *Journal of Geophysical Research*, *115*(D23). https://doi.org/10.1029/2010JD013863

Saunders, C. P. R. (1993). A review of thunderstorm electrification processes. *Journal of Applied Meteorology*, *32*(4), 642–655. https://doi.org/10.1175/1520-0450(1993)032<0642:AROTEP>2.0.CO;2

Sherwood, S. C., Phillips, V. T., & Wettlaufer, J. S. (2006). Small ice crystals and the climatology of lightning. *Geophysical Research Letters*, *33*(5), L05804. https://doi.org/10.1029/2005GL025242

Steiger, S. M., Orville, R. E., & Huffines, G. (2002). Cloud-to-ground lightning characteristics over Houston, Texas: 1989–2000. *Journal of Geophysical Research*, *107*(D11), ACL-2. https://doi.org/10.1029/2001JD001142

Stolz, D. C., Businger, S., & Terpstra, A. (2014). Refining the relationship between lightning and convective rainfall over the ocean. *Journal of Geophysical Research: Atmospheres*, *119*(2), 964–981. https://doi.org/10.1002/2012JD018819

Takahashi, T. (1978). Riming electrification as a charge generation mechanism in thunderstorms. *Journal of the Atmospheric Sciences*, *35*(8), 1536–1548. https://doi.org/10.1175/1520-0469(1978)035<1536:REAACG>2.0.CO;2
Tan, Y. B., Peng, L., Shi, Z., & Chen, H. R. (2016). Lightning flash density in relation to aerosol over Nanjing (China). *Atmospheric Research*, *174*, 1–8. https://doi.org/10.1016/j.atmosres.2016.01.009
Thornton, J. A., Virts, K. S., Holzworth, R. H., & Mitchell, T. P. (2017). Lightning enhancement over major oceanic shipping lanes. *Geophysical Research Letters*, *44*(17), 9102–9111. https://doi.org/10.1002/2017GL074982
Twomey, S. (1977). The influence of pollution on the shortwave albedo of clouds. *Journal of the Atmospheric Sciences*, *34*(7), 1149–1152. https://doi.org/10.1175/1520-0469(1977)034<1149:TIOPOT>2.0.CO;2
Waliser, D. E., & Gautier, C. (1993). A satellite-derived climatology of the ITCZ. *Journal of Climate*, *6*(11), 2162–2174. https://doi.org/10.1175/1520-0442(1993)006<2162:ASDCOT>2.0.CO;2
Wang, B., Huang, F., Wu, Z., Yang, J., Fu, X., & Kikuchi, K. (2009). Multi-scale climate variability of the South China Sea monsoon: A review. *Dynamics of Atmospheres and Oceans*, *47*(1–3), 15–37. https://doi.org/10.1016/j.dynatmoce.2008.09.004
Wang, Q., Li, Z., Guo, J., Zhao, C., & Cribb, M. (2018). The climate impact of aerosols on the lightning flash rate: Is it detectable from long-term measurements? *Atmospheric Chemistry & Physics*, *18*(17), 12,797–12,816. https://doi.org/10.5194/acp-18-12797-2018
Westcott, N. E. (1995). Summertime cloud-to-ground lightning activity around major midwestern urban areas. *Journal of Applied Meteorology*, *34*(7), 1633–1642. https://doi.org/10.1175/1520-0450-34.7.1633
Williams, E. (2020). Lightning and climate change. In A. Piantini (Ed.), *Lightning interaction with power systems volume 1: Fundamentals and modelling* (pp. 1–45). London, UK: Institution of Engineering and Technology.
Williams, E., Chan, T., & Boccippio, D. (2004). Islands as miniature continents: Another look at the land-ocean lightning contrast. *Journal of Geophysical Research*, *109*(D16). https://doi.org/10.1029/2003JD003833
Williams, E., Rosenfeld, D., Madden, N., Labrada, C., Gerlach, J., & Atkinson, L. (1999). The role of boundary layer aerosol in the vertical development of precipitation and electrification: Another look at the contrast between lightning over land and over ocean, 11th International Conf. On Atmospheric Electricity, Guntersville.
Williams, E. R. (1989). The tripole structure of thunderstorms. *Journal of Geophysical Research*, *94*(D11), 13,151–13,167. https://doi.org/10.1029/JD094iD11p13151
Williams, E. R., & Stanfill, S. (2002). The physical origin of the land-ocean contrast in lightning activity. *Comptes Rendus Physique*, *3*, 1277–1292. https://doi.org/10.1016/S1631-0705(02)01407-X
Williams, E. R., Zhang, R., & Rydock, J. (1991). Mixed-phase microphysics and cloud electrification. *Journal of the Atmospheric Sciences*, *48*(19), 2195–2203. https://doi.org/10.1175/1520-0469(1991)048<2195:MPMACE>2.0.CO;2
Yuan, T., Remer, L. A., Pickering, K. E., & Yu, H. (2011). Observational evidence of aerosol enhancement of lightning activity and convective invigoration. *Geophysical Research Letters*, *38*(4), 155–170. https://doi.org/10.1029/2010GL046052
Zhu, Y., Rakov, V. A., Tran, M. D., Stock, M. G., Heckman, S., Liu, C., et al. (2017). Evaluation of ENTLN performance characteristics based on the ground truth natural and rocket-triggered lightning data acquired in Florida. *Journal of Geophysical Research: Atmospheres*, *122*(18), 9858–9866. https://doi.org/10.1002/2017JD027270

References From the Supporting Information

Riggs, G. A., Hall, D. K., & Román, M. O. (2017). Overview of NASA's MODIS and visible infrared imaging radiometer suite (VIIRS) snow-cover earth system data records. *Earth System Science Data*, *9*(2), 765–777. https://doi.org/10.5194/essd-9-765-2017

Geophysical Research Letters

Supporting Information for

Aerosol Effects on Lightning Characteristics: A comparison of polluted and clean regimes

Y. Liu [1], A. Guha [2], R. Said [3], E. Williams [1], J. Lapierre [4], M. Stock [4], and S. Heckman [4]

[1] Department of Civil and Environmental Engineering, Massachusetts Institute of Technology, Cambridge, Massachusetts, USA

[2] Department of Physics, Tripura University, Agartala, Tripura, India

[3] Vaisala Inc., Louisville, Colorado, USA

[4] Earth Networks, Germantown, Maryland, USA

• Lightning response to added aerosol in convectively active seasons

Wet seasons are characterized by active convection favorable for lightning and occurs locally from May to October during the period 2017-2018. The total stroke density maps during the wet seasons are illustrated in Figure S1. Both the IC and CG stroke densities are enhanced significantly over the polluted region with elevated SO_2 column mass density and AOD_{550} during the convective seasons (Figure S1a and S1b). The maximum lightning enhancement lies near the center of the enclosing box for the polluted region. Some gaps with fewer IC and CG strokes can be clearly observed between the polluted region and the coastline, suggesting there is little influence on lightning activity from continent or coasts. Lightning is sparse over the referenced clean region and quantitatively consistent with other open oceanic regions in the southern South China Sea through the wet seasons (Figure S1c-e). This aerosol perturbation on lightning activity concentrates locally and the neighboring regions are not disturbed, thereby showing a satisfactory consistency with the analyses on the annual timescale. All these results in different time resolutions support a noticeable lightning enhancement over the localized polluted ocean for both the IC and CG strokes in comparison with the adjacent clean counterpart.

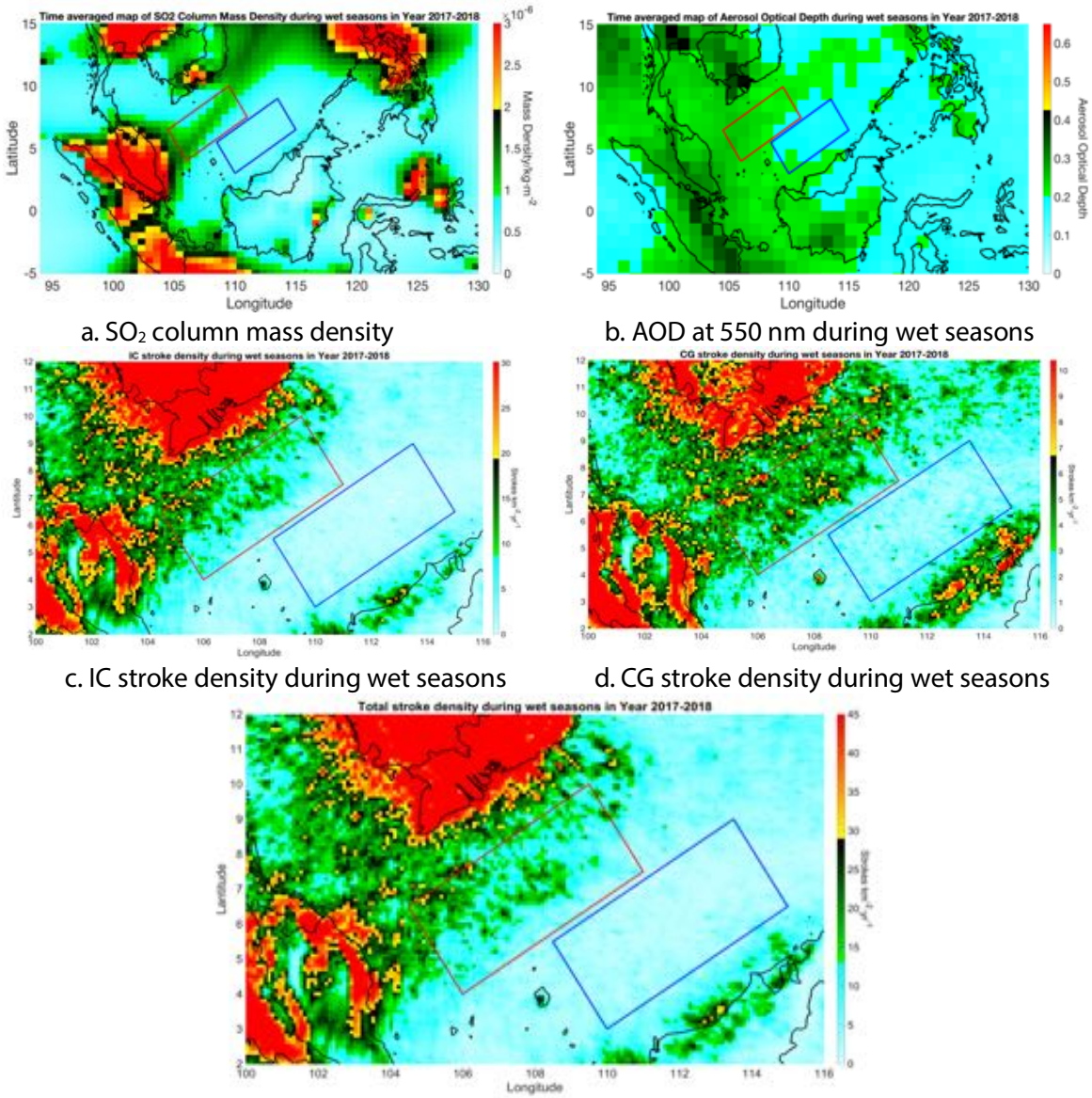

a. SO_2 column mass density

b. AOD at 550 nm during wet seasons

c. IC stroke density during wet seasons

d. CG stroke density during wet seasons

e. Total stroke density during wet seasons

Figure S1. SO_2 column mass density, AOD_{550}, and stroke density during the wet seasons in the period 2017-2018 over the southern South China Sea. The polluted oceanic region is marked with a red box. Its adjacent pristine ocean region is marked with a blue box.

- **An anomaly of AOD_{550} data in August 2018 over the clean oceanic region**

The aerosol optical depth at 550 nm (AOD_{550}) is an aerosol index used to characterize the air pollutants over the ocean [*Andreae*, 2009]. As shown in Figure 1b (in the manuscript, cited here), the biennial average AOD_{550} value changes from 0.19 over the clean region to an average of 0.26 over the polluted region. In the checking of the monthly variations of the AOD_{550} data, the result shows an anomaly in the spike in August 2018 over the clean region (see Figure 3d in the manuscript, cited here). We examined the monthly spatial distribution of AOD_{550} over the South China Sea and its surrounding continent from the database of MODIS

(Collection 6, Level 3, Grid 1×1°) [*Remer et al.*, 2008]. It is found that this AOD_{550} anomaly is caused by aerosol emanating from a strong pollution source over the land near West Kalimantan, Indonesia, as shown in the Figure S2. The strong aerosol source over the land near West Kalimantan, Indonesia is traced to a large number of forest fires and can be clearly verified in Figure S3. The fire count data is derived from the NASA Fire Information for Resource Management System (FIRMS) database (see https://firms.modaps.eosdis.nasa.gov). The FIRMS is capable of monitoring hotspots in Near Real-Time (NRT) and has provided information on active fire data within 3 hours of the satellite observation (including an approximate location of a detected hotspot) from NASA's MODIS and Visible Infrared Imaging Radiometer Suite (VIIRS) instruments for more than a decade [*Riggs et al.*, 2017]. In addition, the wind during August 2018 is mainly from south to north over the West Kalimantan and carries the coastal aerosol to the clean region (Information on wind direction can be found in the database of the Global Forest Watch Fires, http://fires.globalforestwatch.org/map).

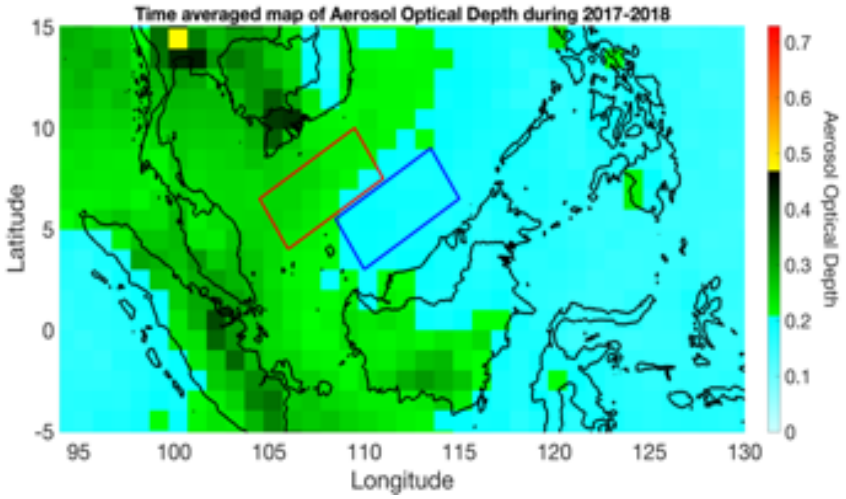

Figure 1b. AOD_{550} (spatial resolution 1×1°) over the south SCS during 2017-2018. The polluted oceanic region is marked with a Red box. The adjacent pristine oceanic region is marked with a Blue box.

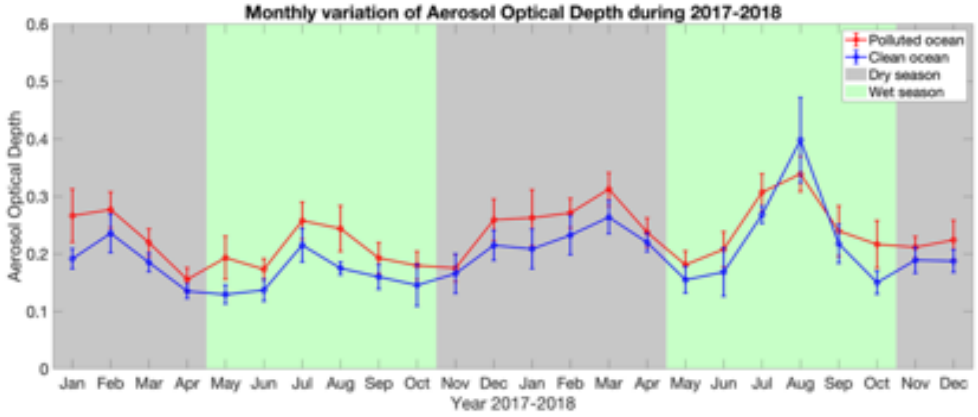

Figure 3d. Monthly variations of AOD_{550} averaged within the polluted region (red line with ± 50% standard deviation at each data point within the region) and its adjacent clean region (blue line with ±50% standard deviation at each data point within the region) during 2017-

2018. Time periods filled with the light gray color show the dry season and the light green color show the wet season.

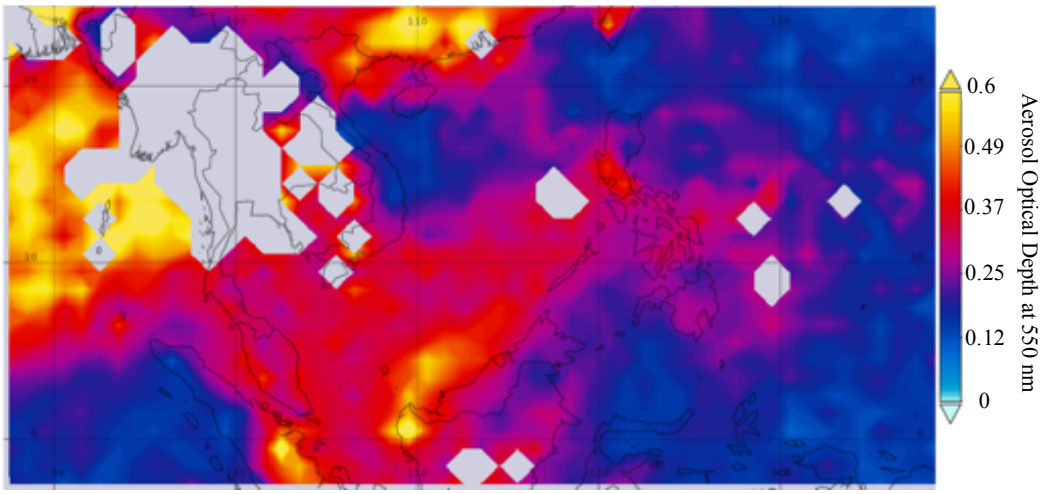

Figure S2. Time-averaged AOD_{550} over the South China Sea and its surrounding continent during August 2018 (from MODIS-Aqua; collection 6, Level 3, smoothed plotting on Grid 1×1°)

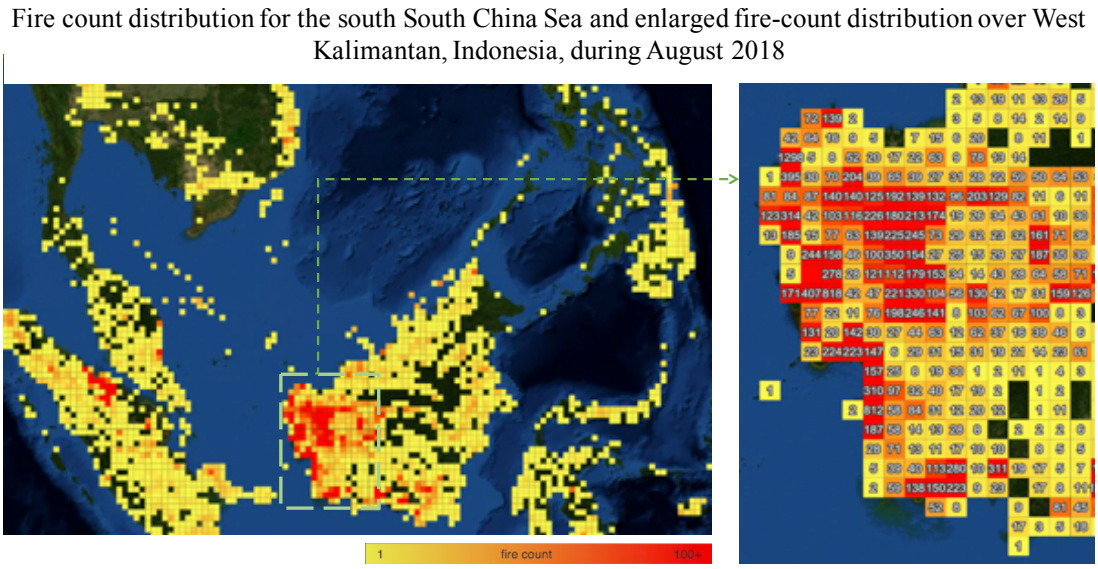

Figure S3. Fire count distribution for the southern South China Sea and enlarged fire-count distribution over West Kalimantan, Indonesia, during August 2018, derived from the NASA Fire Information for Resource Management System (FIRMS) database. This result is documented by the Visible Infrared Imaging Radiometer Suite (VIIRS) instruments.

Acknowledgements

We acknowledge the use of data products and imagery from the Land, Atmosphere Near real-time Capability for EOS (LANCE) system operated by NASA's Earth Science Data and Information System (ESDIS) with funding provided by NASA Headquarters.

References

Andreae, M. O. (2009). Correlation between cloud condensation nuclei concentration and aerosol optical thickness in remote and polluted regions. Atmospheric Chemistry and Physics, 9(2), 543-556. https://doi.org/10.5194/acp-9-543-2009.

Remer, L. A., Kleidman, R. G., Levy, R. C., Kaufman, Y. J., Tanré, D., Mattoo, S., Martins, J.V., Ichoku, C., Koren, I., Yu, H.B., & Holben, B. N. (2008). Global aerosol climatology from the MODIS satellite sensors. Journal of Geophysical Research: Atmospheres, 113(D14). https://doi.org/10.1029/2007JD009661

Riggs, G. A., Hall, D. K., & Román, M. O. (2017). Overview of NASA's MODIS and visible infrared imaging radiometer suite (VIIRS) snow-cover earth system data records. Earth System Science Data, 9(2), 765-777. https://doi.org/10.5194/essd-9-765-2017